De Luca, F., Verderame, G. M., & Manfredi, G. (2014). Eurocode-based seismic assessment of modern heritage RC structures: The case of the Tower of the Nations in Naples (Italy). Engineering Structures, 74, 96-110. 10.1016/j.engstruct.2014.05.015

Eurocode-based seismic assessment of modern heritage RC structures: the case of the *Tower of the Nations* in Naples (Italy)

Flavia De Luca[1], Gerardo M. Verderame, Gaetano Manfredi

Department of Structures for Engineering and Architecture, DiSt, University of Naples Federico II, Via Claudio, 21, 80125 Naples

ABSTRACT

Given the interest earned recently by modern heritage structures, seismic assessment criteria of Eurocode 8 for ordinary reinforced concrete structures are applied to a modern heritage RC building. The case study building, the Tower of the Nations in Naples, was designed at the end of 30's. Modal dynamic identification, *in situ* inspections and testing provided the necessary knowledge of the structure in terms of geometry, structural details, and material properties. Two nonlinear models of the structure are built up in both the hypotheses of accounting and not accounting for tuff infills' stiffness and strength contribution. Lumped plasticity model for reinforced concrete elements and equivalent strut models for tuff and concrete infills are employed. Seismic assessment through nonlinear dynamic analyses is carried out for both Damage Limitation and Significant Damage limit states. Assessment of bare and infilled models emphasizes a lower demand in terms of maximum interstorey drift of the infilled model with respect to the bare model, for both limit states considered. Record-to-record variability for the sets of seven records becomes larger if infills strength and stiffness contribution is taken into account. The outcome of the assessment is not affected by infills, i.e. the structure can be considered safe (according to EC8 provisions) for both limit states, and in both modeling hypotheses. On the other hand, the demand over capacity ratio, for both the limit states considered, is strictly influenced by infills' contribution. Results provided show that Eurocode assessment tools for ordinary RC structures can be addressed to modern heritage buildings, even if specific care is necessary for nonlinear structural modeling in case of non-conventional structural elements and non-conventional structural materials (e.g., tuff infills in lieu of clay hollow brick infills).

Keywords: *modern heritage structures, seismic assessment, RC building, tuff infills, nonlinear dynamic analysis*

1. INTRODUCTION

A first definition of the concept of *heritage*, and, in turn, of *heritage buildings* was provided in the Charter of Venice (1964), in which it is stressed, not only the value of the message from the past, but also the common responsibility to their safeguard for future generations, [1]. On the other hand, within heritage buildings, a distinction can be made between historical buildings and monumental buildings. The former are those that can be defined as buildings of artistic or cultural value, and which are found in significant numbers; the latter are those truly unique, [2].

One of the criteria that classifies heritage or historical structures is that long time has passed since their construction, [3]. On the other hand, "old" is a relative term, and, in practice, can be as low as 50-100 years. As an example, the definition of architectural heritage is experiencing an evolution in time. In particular, the category of *modern heritage structures* is earning increasing interest (e.g., [4], [5]). Hence, more and more reinforced concrete (RC) structures can be classified

[1] Corresponding author: flavia.deluca@unina.it - tel. +390817685959 - fax +390817685921

in this category, although RC is a rather new structural material in comparison with wood and bricks.

In the above framework, seismic assessment of modern heritage structures is an issue that earns interest in seismically prone regions in Europe, such as Italy, Greece, Portugal or Turkey (e.g., [6]). The uniqueness characteristic of heritage buildings requires specific assessment approaches [2], often ruled by specific guidelines in the different countries (e.g., [7]). Thus, it is rare to find code approaches for ordinary structures employed for the assessment of heritage buildings. On the other hand, the case of modern heritage RC buildings allows addressing seismic assessment provisions, meant for ordinary structures, to this category.

Herein, an example of Eurocode or EC8 based assessment [8] performed for a modern heritage RC building is provided. Notwithstanding the fact that general assessment principles for ordinary RC structures can be easily applied to modern heritage buildings; this kind of buildings often are structurally very peculiar and therefore they require significant modeling efforts and accurate analysis methodologies.

The *Tower of the Nations* is a modern heritage structure, located within the Mostra d'Oltremare urban park in Naples [9]. The whole urban park was nominated in 2005 for the inscription in the UNESCO Modern Heritage List (http://whc.unesco.org/en/events/247/), given its relevant expression of the cultural and technical background at the time of design and construction. The Tower of the Nations was designed in 1938 by the architect Venturino Ventura, with the help of Carlo Cestelli Guidi, one of the most important structural engineers at the time, and of the architect and painter Guido Quaroni. The building was completed in 1940. The Tower has two glazed façades without any masonry infills, to stress the ideal continuity with the main square of the park, and it has the other two façades fully infilled by tuff masonry, covered by white travertine plates to make visible the imposing volume of the Tower, see Figure 1. In 1940, the building had a basement decorated with low reliefs and a big statue representing the Fascist Victory (see Figure 1a); the provisional chalk version of the low reliefs was destroyed during the Second World War.

In the years following its construction, the structure was left to the carelessness. Recently the Tower has been included in the project of restoring the entire Mostra d'Oltremare urban park. The project includes the assessment and retrofitting of the Tower.

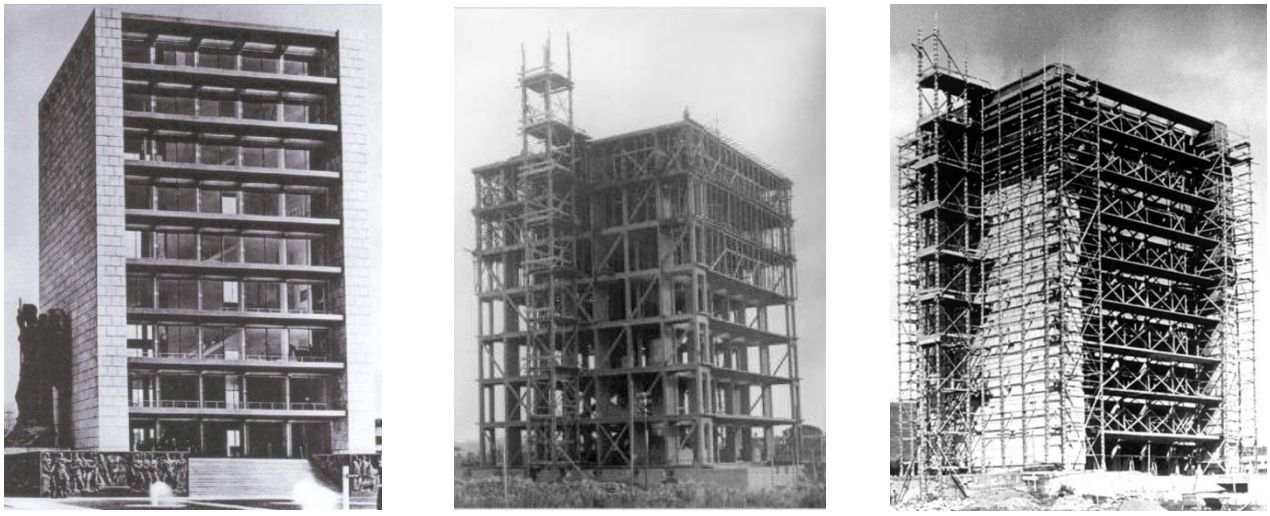

(a) (b) (c)

Figure 1.Tower of the Nations: (a) completed, (b) and (c) under construction.

Herein, the assessment of the structure follows EC8 framework, [8]. Thus, firstly all the required input data for the assessment are collected, considering, respectively, *geometry*, *details* and *materials* (section 2). Then, modeling issues, and linear and nonlinear models of the structure are described in section 3. Finally, assessment is carried out for *Significant Damage* (SD) and *Damage Limitation* (DL) Limit States by means of nonlinear dynamic analyses (section 4). All the analyses

are carried out for both the bare model of the Tower and the tuff infilled one, comparing results in terms of interstorey drift ratio (IDR).

2. KNOWLEDGE OF THE STRUCTURE

Input data for the assessment of existing structures shall be collected from a variety of sources, including: available design documentation of the building, relevant generic data sources (e.g. codes and standards at the time of construction), *in situ* investigations, and laboratory tests. EC8 provides a quantitative framework for the definition of *knowledge levels* of structures in order to choose the admissible type of analysis and the appropriate confidence factor to be employed in the assessment.

In this case, study, the main purpose is to carry out the assessment of the Tower of the Nations through nonlinear dynamic analysis. According to EC8 prescriptions, a *normal knowledge level* (KL2) is required for the assessment of structures through nonlinear analysis approaches. Knowledge level of an existing structure is determined by three factors: *geometry*, *details*, and *materials*.

Following the path suggested by EC8, the whole geometry of the structural system is described in section 2.1. A brief description of *in situ* inspections and the simulated design procedure aimed at determining reinforcements in beams and columns is provided in section 2.2. Finally, material properties and *in situ* testing are described in section 2.3.

2.1 Geometry

Geometry was retrieved from the original architectural drawings, and thanks to a structural survey, see Figure 2 and 3. The Tower of the Nations is characterized by ten storeys, 44.00 meters tall, and it has a roughly square plan (Figure 2). It is 23.50 m long in North-South direction (in the following Y direction), and 23.70 m wide in the other direction (X direction), see Figure 3. The structure has a system of staggered floors that occupies only one-half of the plan from levels forth to ninth (see Figure 2a, Figure 3d, 3e).

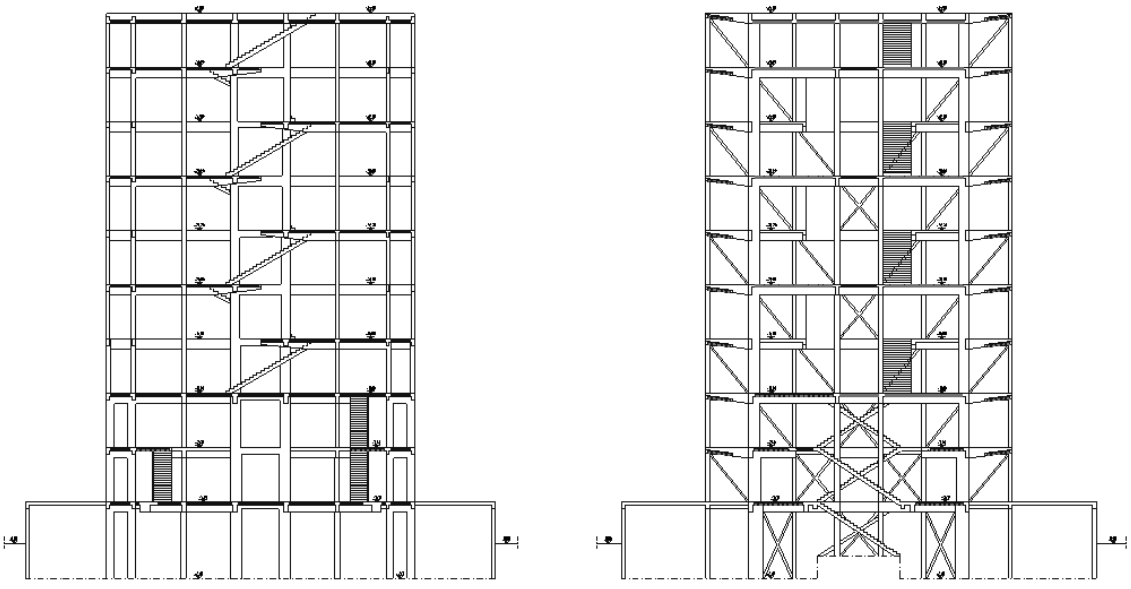

(a) (b)

Figure 2. Tower of the Nations: (a) transversal (XZ); (b) longitudinal (YZ) sections

Considering the fact that Naples was not classified as seismic zone, the structure should have been designed for gravity loads only according to code prescription for RC structures at the time ([10], [11]). On the other hand, the peculiarities of the structural system show that horizontal forces, probably wind action, were taken into account in the design.

The structural system of the Tower is very innovative considering the age of construction. The building is characterized by a three-dimensional frame system. Two couples of frames (seven bays) are placed at two opposite sides of the plan (along Y-Z plane). They are coupled each other by squat beams, 1.80 m long, with a cross section of 300×800 mm^2. The two frames on East and West façades (YZ) are stiffened by a concrete bracing system. Concrete bracings alternatively occupy the bays of the prospect frames from first to eighth level, see Figure 2b. In this direction (YZ), there are also tuff masonry infills without openings. In X direction, the structural system is composed by different schemes of frames, with different number of bays. Frame system in this direction is integrated by slim concrete walls situated at the centre of the plan (lift-shaft) and at the two sides of the plan in X direction. Along X direction there are no masonry infills.

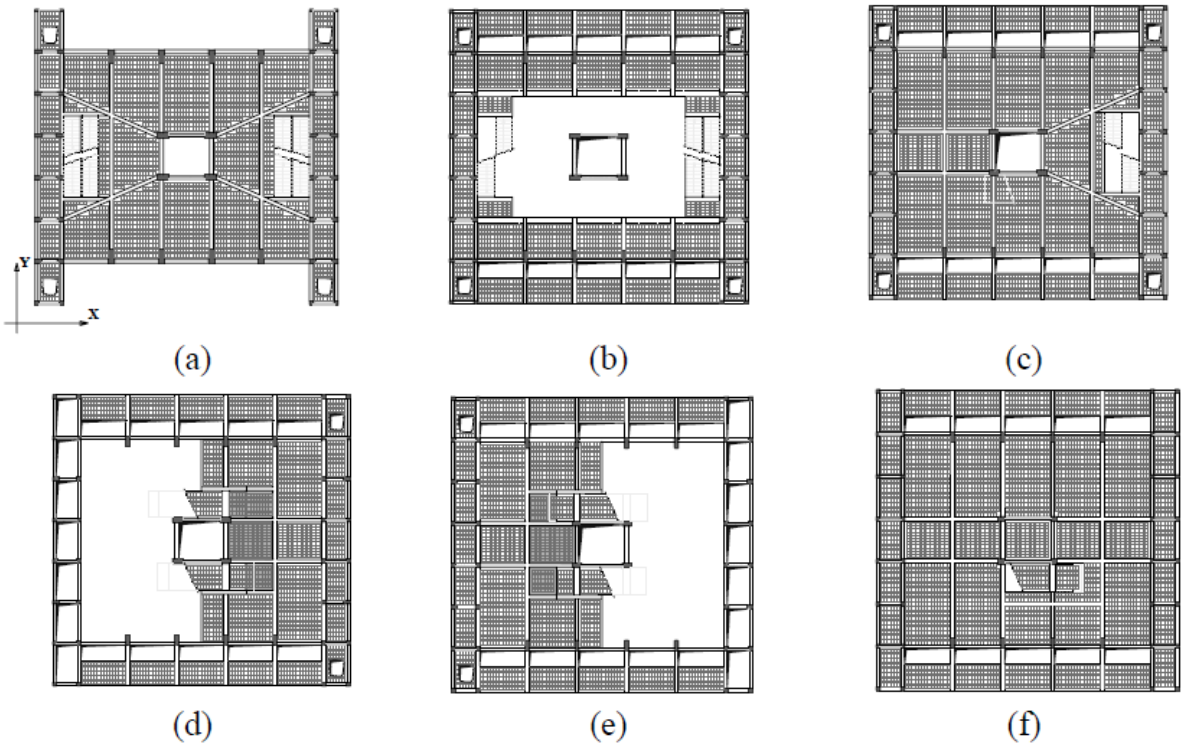

Figure 3.Tower of the Nations: structural drawings (a) first level plan; (b) second level plan; (c) third level plan; (d-e) typical plan; (f) tenth level plan.

The Tower has a concrete basement, 36.50m long in Y direction, and 36.00 m large in X direction (see Figure 2). Two flights of stairs allow the access to the first storey from ground level, (see Figure 1a). Foundations are characterized by isolated footings with poles. Interstorey height is 4.20m, with the exception of the first storey, whose height is 5.90m, (footings are located at -2.70m from ground level).

Along the ten storeys, the Tower presents different plan configurations. The first storey (Figure 3a) is a "full plan story"; slabs occupy all plan space with stairs placed along Y direction. It presents four diagonal beams that link the lift-shaft with the seven-bay frames in Y direction. The second storey (Figure 3b) is the only storey not linked with the lift-shaft by any beam; it has a landing slab along the perimeter of the plan and it has two staircases continuing from the first level (along Y direction). The third storey (Figure 3c), as well as the first one, is a "full plan story" with two staircases. One of them is placed on the East side of the plan, along Y direction (replicating stairs' position at first and second levels), and the other staircase is a single ramp placed on the South side of the plan, along X direction (see also Figure 3d).

From fourth to ninth storey (Figure 3d, 3e) slabs occupy alternatively only half of the plan; they staggered with respect to Y direction. Stairs at the staggered floors are adjacent to the lift-shaft, and placed along X direction. Tenth level (Figure 3f) is, again, a "full plan story". It is worth noting

that staircases represent the main connection between staggered storeys and they couples "half plan" storeys, see Figure 2a.

Structural *in situ* survey and symmetry in plan allowed a full knowledge of beams and columns' sizes. Every storey has 44 columns, mostly located along the perimeter of the plan. Columns' sections are rectangular; they are oriented with the strong axes along Y direction, and placed in the two principal frames in X direction. Sections change from the values 450×1100 mm^2 at the first storey to 300×800 mm^2 at the tenth storey. In the lift-shaft, rectangular columns have the strong axes in X direction; sections vary from 900×400 mm^2 at first storey, to the 500×400 mm^2 at tenth storey. Concrete walls thickness is 150mm in the lift-shaft and 100mm for elements in the lateral zone of the frames in X direction.

Beam sections vary from 250×500 mm^2, for elements placed in the seven-bay frames along Y direction, to 300×800 mm^2 for elements that connect the lift-shaft with the lateral seven bay frames in the two directions. Wide beams' sections at the second storey are 500×220 mm^2.

One way RC slabs have 180 mm thick joists, and 50 mm of full concrete slab. Stairs are realized with full concrete slabs (230mm thick). Full concrete slabs (230mm thick) are also placed close to the stairs and close to the lift-shaft at each staggered floor.

2.2 Details

Structural details, such as amount and detailing of reinforcement in the RC elements are obtained by *in situ* inspections (Figure 4) and through non-destructive methods. Simulated design is carried out aimed at integrating information from inspections for longitudinal reinforcement of beams [12]. Footings dimensions have been determined through *in situ* survey (Figure 4a). Stirrups in beams and columns are characterized by 6mm diameter and spaced at 250mm, see Figure 4b, while shear reinforcement in beams is characterized by both stirrups (Figure 4c) and diagonal reinforcements at the ends of the elements. Symmetry in plan of the structure along both axes allowed determining structural details of all RC elements.

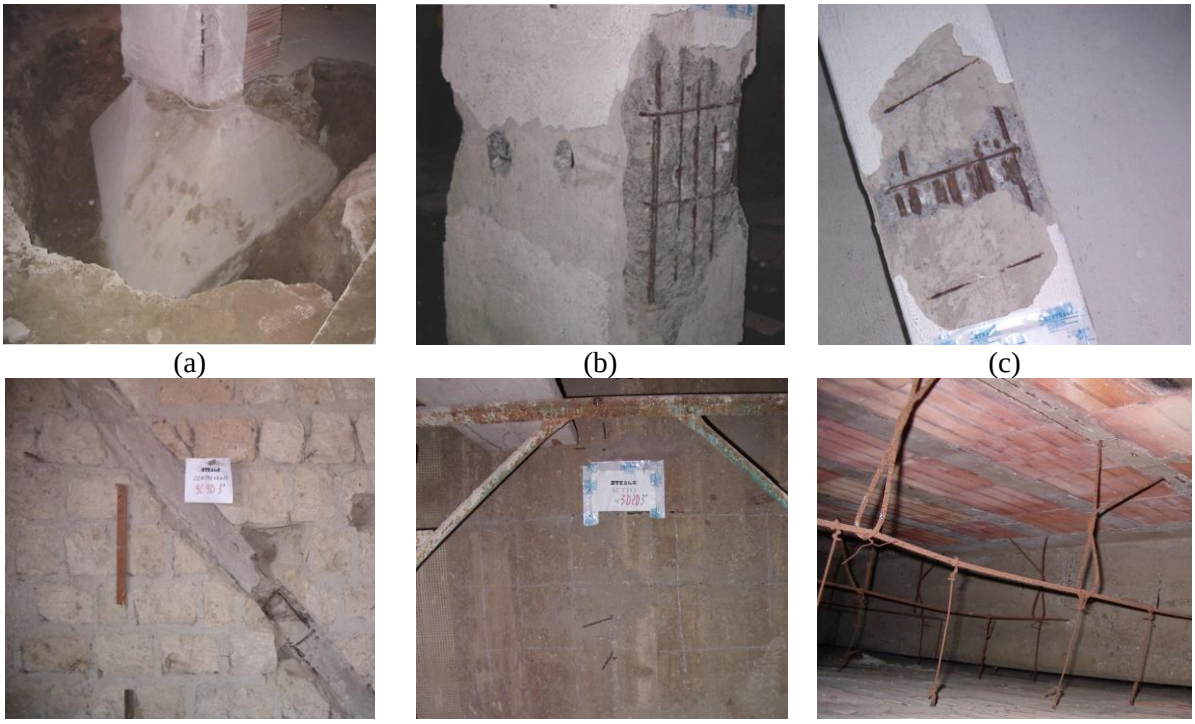

(a) (b) (c)

(d) (e) (f)

Figure 4. In situ inspections: (a) foundation footing; (b) columns' and (c) beams' reinforcement; (d) concrete diagonal brace in tuff masonry infill; (e) concrete infill; (f) floor slabs.

In situ inspections have been performed on RC braces (Figure 4d) and concrete infillings (Figure 4e). RC braces have rectangular sections (350×150mm^2); and their longitudinal

reinforcement is characterized by four bars whose diameter is 10mm. Slim concrete walls are characterized by very poor reinforcement (diameter 10 mm every 300 mm). Joists in floor slabs are 180 mm thick and 400mm spaced (Figure 4f).

2.3 Materials

Material properties are obtained through both destructive and non-destructive tests. Non-destructive test methods are employed in conjunction with destructive tests in accordance with EC8 provisions.

Concrete cylindrical compressive strength (f_{cm}) is evaluated equal to 16MPa from a combination of non-destructive test and from concrete specimens, see Figure 5a. Such value is quite similar to the minimum values of cubic compressive strength of concrete provided by Regio Decreto 27/07/1933 [10], and by Regio Decreto 16/11/1939 [11]. *Ad hoc* calibration of Son-Reb tests is performed according to the procedure suggested for existing RC buildings in Manfredi et al. [13]. Carbonation depth varies significantly in the different concrete specimens; average depth value is equal to 50 mm, (Figure 5b).

Steel mechanical characterization is carried out by collecting specimens from both columns and beams, see Figure 5c. Steel reinforcement is characterized by smooth bars. Significant corrosion of the reinforcement is observed for bars' specimens taken at first and tenth floors. Average yielding strength (f_{ym}) is equal to 275 MPa; again, this value is approximately equal to the minimum value of yielding strength of mild steels provided by Regio Decreto 16/11/1939 [11].

Information on *geometry*, *details*, and *materials* are suitable to achieve a *normal* knowledge level (KL2) for the structure, according to EC8. Confidence factor (CF) was employed to convert average material properties into values to be employed in the assessment procedure. In case of KL2 the CF applied to concrete and steel mechanical properties is equal to 1.20.

(a)

(b)

(c)

Figure 5. In situ testing

3. STRUCTURAL MODELING

Structural modeling of the Tower of the Nations is carried out in two phases. Firstly, linear model is built up aimed at determining modal properties of the structure; secondly, nonlinear model of the Tower is built up. The structural contribution provided by tuff infills is evaluated through the definition of two different modeling approaches for linear and nonlinear behavior.
Loads are defined according to the destination of expository space, following Italian provisions about loads. Masses are uniformly distributed on the slabs.

3.1 Linear model and modal properties

Linear model of the structure is built up using SAP 2000 [14]. The basement is not modeled. It has a negligible interaction with the Tower, and linear dynamic behavior is slightly affected by its presence [15]. Nevertheless, the effect of the two flights of stairs is modeled restraining the degrees of freedom in plan (X, Y) at first storey. Footings are considered as fully restrained joints, not taking into account structure-foundation interactions. Beams, columns and bracings are modeled as elastic mono-dimensional elements (frame).

Slabs, concrete infills, and tuff masonry infills, are modeled as shell element characterized by in-plan behavior only (membrane). Stairs are modeled as thick shell.

Concrete Young modulus (E_c) is assumed equal to 25300 MPa, evaluated as a function of concrete medium compressive strength f_c according to the expression reported in [16]. Tuff infills properties are taken according to the average values reported in [17]; thus, Young modulus (E_w) is equal to 1260 MPa and shear modulus (G_w) is 0.30 times E_w. Figure 6 shows the two different linear models: the bare model, in which there are no tuff infills (see Figure 6a), and the infilled model, in which infills' structural contribution is accounted through shell elements (see Figure 6b).

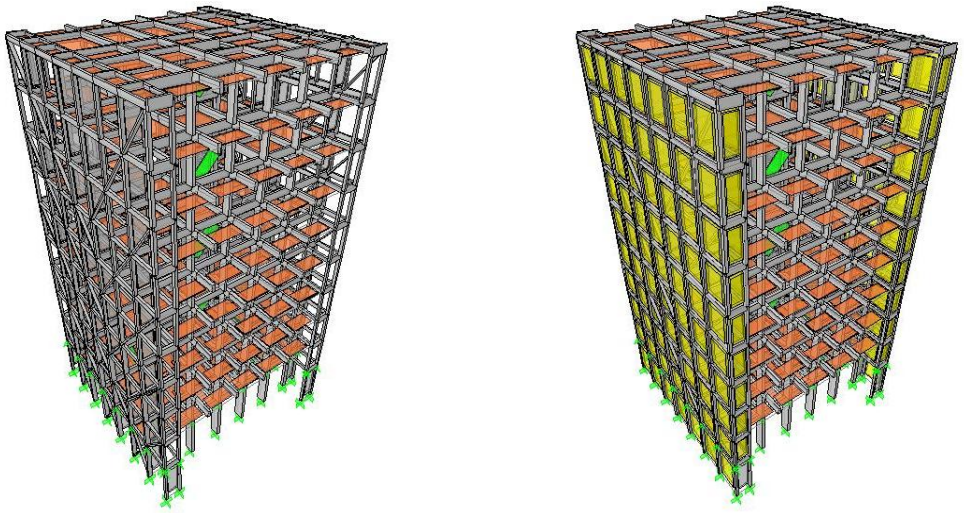

(a) (b)

Figure 6. Geometrical model of the structure without and with tuff infillings.

The two linear models are employed to determine modal properties of the structure. The first three periods and mass participant ratios are shown in Table 1. It is worth noting that tuff infills affect strictly the first translation mode in Y direction (second mode) and the third torsional mode. Linear dynamic properties of the infilled model show a good agreement with experimental results obtained by the dynamic identification made on the building [15]. Both first and second modes in bare and infilled models show a considerable rotational participation mass coefficient (M_{RZ}) that slightly increases when infill stiffness contribution is considered. The first three fundamental periods of the structures resulting from dynamic identification of the structure, provided by Rainieri et al. [15], are linear model accurately captures periods with errors within 6%, and it shows a very accurate match for the second mode (along Y direction).

Table 1. Modal properties for bare frame model and the tuff infilled.

Model	**mode**	**T** [sec]	**M_X**	**M_Y**	**M_{RZ}**
Bare frame	1	1.35	0.65	0.00	0.25
	2	1.10	0.00	0.68	0.28
	3	0.93	0.00	0.00	0.14
Tuff infilled frame	1	1.33	0.65	0.00	0.27
	2	0.74	0.00	0.70	0.30
	3	0.64	0.00	0.00	0.14

3.2 Nonlinear model

Lumped plasticity modeling approach is employed for the two nonlinear models of the Tower. Nonlinear modelling of structural elements (beams, columns, diagonal braces, concrete infills, tuff infills) is carried out using *link* hysteretic elements in SAP2000 [14]. The link element is a nonlinear spring with six independent internal deformations for which a generalized force

deformation nonlinear relationship can be defined. It is used to connect two joints together. In the nonlinear model of the Tower of the Nations, link element has been employed in different ways.

For monodimensional elements with dominant flexural behavior (beams and columns), two finite length links have been placed at the two ends of the frame element. Link elements capture both linear and nonlinear flexural behavior of beams and columns. The frame element is modeled as rigid, thus resulting in a lumped elasticity and plasticity model. For monodimensional elements with dominant axial behavior (concrete braces), two finite length links have been placed at the two ends of the frame element. In this case, the nonlinear axial springs are characterized at the two ends and the other degrees of freedom are released.

For bidimensional nonlinear elements (slim concrete walls and tuff masonry infills), an equivalent strut modeling strategy has been selected. In this case, the link is a nonlinear axial spring that can carry only compression connecting the two opposite corners of the bay in which the bidimensional element is placed. The other degrees of freedom are released. Considering that time-history analysis is characterized by inverting loading, in each frame, there are two of these elements along the two diagonals. Finally, it is worth noting that link elements can be characterized by mass, and in each of the above modeling strategies, the proper mass was assigned to the springs.

In the following, a detailed description of the generalized force deformation nonlinear relationship assumed for each element is provided.

3.2.1 RC columns and beams

Nonlinear behavior of RC columns is represented by a moment-rotation (M-θ) relationship, evaluated *a priori*. In particular, each M-θ is defined through four characteristic points (Figure 7): cracking (cr), yielding (y), maximum (max) and ultimate (u). Cracking, yielding and maximum moments are evaluated for the two principal directions (M_2, M_3) of the sections according to the hypotheses of (i) no biaxial interaction, (ii) no interaction with axial internal force. Axial force was considered as constant during the analysis and equal to that evaluated from the seismic combination of gravity loads. Bending moments of M-θ relationships are evaluated through a fiber analysis of the end sections of each element, assuming an unconfined Mander stress-strain relationship [18] for concrete and an elastic perfectly plastic stress-strain relationship for reinforcement steel. The ultimate moment M_u is determined as M_u=0.80M_{max}, consistently to the corresponding definition of ultimate chord rotation.

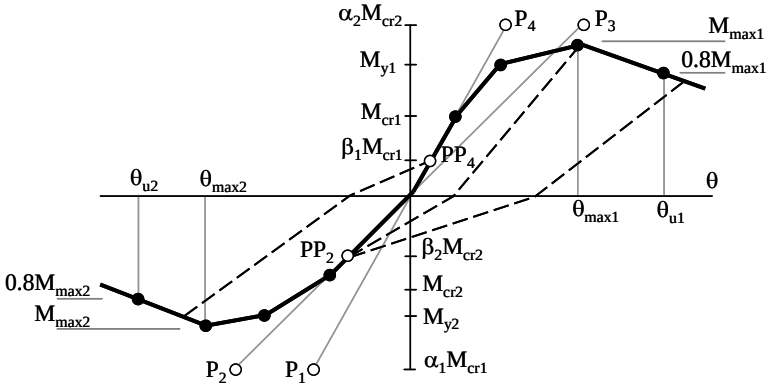

Figure 7. Columns' M-θ backbone and hysteretic behavior

Chord rotations corresponding to each point of the M-θ relationship are evaluated according to literature or experimental results. Yielding and ultimate chord rotations of columns are evaluated according to equations 1 and 2 [8]:

$$\theta_y = \frac{\phi_y \cdot L_V}{3} + 0.0014 \cdot \left(1 + 1.5\frac{h}{L_V}\right) + \phi_y \cdot \frac{d_b \cdot f_y}{8\sqrt{f_c}} \quad (1)$$

$$\theta_u = 0.016 \cdot 0.3^{\nu} \left[\frac{\max(0.01;\omega')}{\max(0.01;\omega)} f_c \right]^{0.225} \left(\frac{L_V}{h} \right)^{0.35} 25^{\alpha\rho_{sx}\frac{f_y}{f_c}} 1.25^{100\rho_d} \quad (2)$$

where:

h	is the depth of cross-section, ν is the normalized axial load,
d_b	is the diameter of longitudinal reinforcement,
ω and ω'	are the mechanical ratios of tension and compression longitudinal reinforcement, respectively,
f_c and f_y	are concrete compressive strength and steel yield strength,
ρ_{sx}	is the ratio of the transverse steel parallel to the direction of loading,
ρ_d	is the steel ratio of diagonal reinforcement, in each diagonal direction,
α	is the confinement effectiveness factor.

The yielding curvature ϕ_y is evaluated through a fiber analysis of the section, while the shear length (the ratio moment/shear at the end section), L_V, is assumed constant and equal to 0.50L, according to a simplified hypothesis. Equation 1 leads to a reliable prediction of the yielding rotation for elements without seismic detailing and reinforced with smooth bars [19]. In the case of ultimate chord rotation (θ_u), a reduction equal to (0.95/1.2) with respect to the value obtained from equation 2 was considered, because of the absence of seismic detailing and the presence of continuous smooth longitudinal bars [20]. On the other hand, the reduction factor assumed for θ_u, seems to provide a conservative estimation in the light of the additional experimental results shown in Verderame et al. [21]. Finally, rotation corresponding to maximum moment (θ_{max}) is evaluated as function of the yielding value (θ_y), according to the experimental results shown in Verderame et al. ([22]; [23]), and Di Ludovico et al. [24].

The model assumed for beams is similar to that assumed for columns. Two main differences characterize beams' M-θ backbone: (i) the backbone is generally non-symmetric, and (ii) M-θ backbone is assumed perfectly plastic after yielding point (M_y=M_{max}=M_u) without any softening. It is worth noting that the mechanical reinforcement ratio in compression and tension (ω'/ω), in equation 2, leads to differences in θ_u values corresponding to positive and negative bending moments.

A hysteretic relationship in strength and stiffness is assumed, see Figure 7. This model is similar to the Takeda et al.'s model [25]; but it has additional parameters ($\bar{\alpha}, \beta, \eta$) to control degrading behavior in the hysteretic loop, [26]. It is well suited for reinforced concrete members, and it is based on the observation that unloading and reverse loading tend to be directed toward specific points, called *pivots points* on the force-deformation (or M-θ) plan [26]. Parameters $\bar{\alpha}$ and β are defined as function of axial load ratio and longitudinal steel ratio, and η, which determines the amount of degradation of the elastic slopes after plastic deformation, is assumed equal to 10.

Brittle failure of columns and beams are excluded *a priori* because shear strengths, evaluated according to EC8 [8], are larger than flexural strengths of these elements. Thus, all columns and beams can be classified to have ductile behavior. These results are expected because columns and beams are characterized by very low longitudinal steel ratios that allow favorable shear-flexure hierarchy [27].

3.2.2 Concrete diagonal braces

Concrete diagonal braces represent one of the peculiar design issues of the structure and they influences strictly the seismic response of the Tower. Concrete struts are characterized by a 350×150mm^2 section, lightly reinforced with four 10mm longitudinal bars. Due to the reduced transversal section dimensions of the concrete bracings, and their poor longitudinal reinforcement, the only axial behavior of these elements is taken into account and modeled.

Two axial springs at the end of each element are considered and no bending moment constraint was assumed at the intersection with beam-column joints. Axial springs of each concrete

diagonal brace are modeled with an elastic perfectly plastic behavior in tension (accounting for the longitudinal reinforcement) and a nonlinear behavior in compression.

The compression behavior of the element is evaluated assuming an unconfined Mander stress–strain relationship for concrete, accounting for the possible buckling of the element through the evaluation of buckling critical tension σ_{crit}. In particular, due to high slenderness of the braces, the buckling critical tension σ_{crit} is lower than concrete compressive strength f_{cm} [28].

A four point force-displacement backbone is assumed for every axial spring (Figure 8) at the two ends of the element. In tension, the maximum axial force (F^{-}_{max}) is evaluated as the product of steel yielding stress (f_{ym}) and steel reinforcement area (A_s). The corresponding displacement Δ^{-}_{max} is assumed as the ratio between F^{-}_{max} and the axial stiffness in tension ($K^{-} = 2E_s A_s / L$), where L is the concrete brace length. Concrete in tension and post cracking tension-stiffening effects are neglected for the evaluation of initial stiffness. First compression characteristic point is characterized by the axial force (F^{+}_{max}), computed as the product of concrete section area (A_c) and σ_{crit}, while the corresponding drop displacement Δ^{+}_{max} is assumed as the ratio between F^{+}_{max} and the axial stiffness in compression ($K^{+} = 2E_c A_c / L$). The second point in compression is considered in correspondence of zero axial force and displacement Δ^{+}_{max}. Takeda et al.'s hysteretic model [25] is assumed.

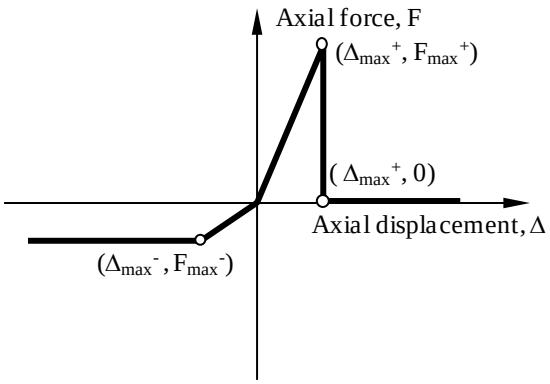

Figure 8. Diagonal braces' force-deformation envelope

It is worth noting that concrete bracings are placed on the façades in which are present also tuff masonry infills. The interaction between concrete bracing and tuff infills is not taken into account; the interstorey drift ratio (IDR), which corresponds to the maximum strength of the tuff infillings, is lower than the IDR that corresponds to the instability due to axial load in compression of the concrete struts. Thus, it is assumed that the infill cannot restrain the occurrence of buckling in the bracing, given the extensive damage that corresponds to the softening phases of infills' backbone. Furthermore, when a concrete brace is present in the frame, the corresponding link, modeling the tuff (infill) equivalent strut element in that direction is not modeled (see also section 3.2.3).

3.2.3 Tuff and concrete infillings

Tuff and concrete infills are modeled through an equivalent strut macro-model [29]. They are two crossing diagonal axial springs (link) that can carry compression only. Equivalent struts width (b_w) is determined by equation 3 [30], being h_w infills' height, L_w their length in plan; d_w is $\sqrt{h_w^2 + L_w^2}$, and λ is calculated according to equation 4.

$$\frac{b_w}{d_w} = 0.175 \cdot (\lambda \cdot h_w)^{-0.4} \tag{3}$$

$$\lambda = \sqrt[4]{\frac{E_w \cdot t_w \cdot \sin(2\cdot\theta)}{4 \cdot E_c \cdot I_p \cdot h_w}} \quad (4)$$

In equation 4, the inclination angle θ of the strut is equal to *arctan*(h_w/L_w), E_w and E_c are, in this case, respectively equal to tuff and concrete Young modulus, I_p is the inertia of the columns of the bay in which the infill is placed, finally, t_w is the thickness of the infill. Tuff infill backbone has three characteristic points (Figure 9a):

(i) *cracking point* (F_{cr}, Δ_{cr}), force is assumed as the product of shear cracking stress(τ_0) and the area of the infill ($t_w \cdot L_w$), while displacement is defined as the ratio between F_{cr} and the shear stiffness K_{el} (=$G_w \cdot L_w \cdot t_w/h_w$), both transformed along the diagonal direction;

(ii) *maximum point* (F_{max}, Δ_{max}), force is assumed as $1.3 \cdot F_{cr}$, and displacement is equal to the ratio between F_{max} and the equivalent strut axial stiffness $E_w \cdot t_w \cdot b_w / d_w$;

(iii) *ultimate point* (F_u, Δ_u), force is assumed as 5% of the maximum strength, and displacement is computed assuming a softening stiffness equal to ($0.01 \cdot K_{el}$). Infills' backbone is evaluated assuming E_w=1260 MPa, τ_o=0.04 MPa [17], infills' shear modulus (G_w) equal to $0.30E_w$, and E_c=25300 MPa.

Takeda et al.'s hysteretic model [25] is assumed for tuff infill panels. It is worth noting that tuff infills in bays with diagonal bracings are not modeled in the direction of the braces.

Tuff infills are characterized by an unusual shape factor with respect to typical practice in ordinary RC buildings; in fact, h_w is higher than L_w. According to the latter observation, the consistency of the strut mechanism is verified through an empirical formulation [31], resulting from experimental studies on brick and concrete infilled non-ductile frames (see equation 5).

$$\frac{f'_m}{\tau_o}\frac{n_1 h_w}{n_2 t_w} > 36 \quad (5)$$

In equation 5, n_1 is the number of bays (seven in the case of the Tower), n_2 is the number of storeys (ten in the case of the Tower), f'_m is infills' compressive strength. When condition in equation 5 is satisfied, the infill panel should fail because of strut mechanism.

Due to their poor longitudinal reinforcement and their limited thicknesses (100 mm lateral; 150 mm in the lift–shaft zone), concrete walls are treated as *concrete infills*. The only shear stiffness is considered, and a strut macro-model is assumed, in analogy with that assumed for tuff infills.

Equivalent strut width is determined according to equations 3 and 4. In this case, E_w is equal to E_c, and G_w is the concrete shear modulus, equal to 10600 MPa. Shear cracking stress τ_o is equal to 0.3 MPa.

Concrete infills' backbone is evaluated through the same modeling hypothesis made for tuff infills. Maximum point estimate (F_{max}, Δ_{max}) is also compared with experimental results ([31], [32], [33]). Concrete infills' model has three characteristic points (Figure 9b):

(i) *cracking point* (F_{cr}, Δ_{cr}), force is assumed as the product of τ_o, t_w and L_w, and displacement is defined as the ratio between F_{cr} and shear stiffness ($G_w \cdot L_w \cdot t_w/h_w$), both transformed along the diagonal direction;

(ii) *maximum point* (F_{max}, Δ_{max}), force is the product of f_{cm} and the area of the equivalent strut ($b_w \cdot t_w$), while displacement is equal to 2‰ of strut's length d_w;

(iii) *ultimate point* (F_u, Δ_u), force is 5% of the maximum strength, and displacement computed assuming a softening stiffness equal to ($0.01\ K_{el}$).

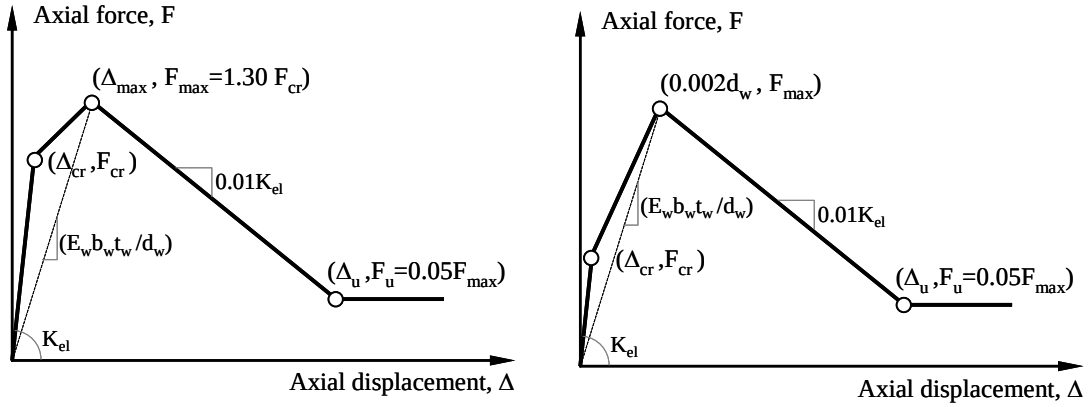

Figure 9. Force-displacement envelope scheme – (a) tuff infills; (b) concrete infills.

4. NONLINEAR DYNAMIC ANALYSIS and ASSESSMENT

Assessment through nonlinear dynamic analysis requires proper seismic input selection. Seismic input has to reflect hazard analysis results and structure's site characteristics. According to EC8 part 1 [34], the description of ground motion may be made by using artificial, recorded or simulated accelerograms. In this case, study, a set of linearly scaled recorded accelerograms was chosen for each limit state: *Significant Damage* (SD-LS), *Damage Limitation* (DL-LS).

EC8 [34] recommends average spectral matching of the records and the main criteria for selection are:

(i) a minimum of 3 accelerograms should be used;

(ii) the mean of the zero period spectral response acceleration values (calculated from the individual time histories) should not be smaller than the value of $a_g \cdot S$ (being a_g the peak ground acceleration, and S the soil amplification factor for the site);

(iii) in the range of periods between $0{,}2T_{el}$ and $2T_{el}$ (being T_{el} the fundamental period of the structure in the direction in which the accelerogram is applied), no value of the mean 5% damping elastic spectrum, calculated from all time histories, should be less than 90% of the corresponding value of the 5% damping elastic response spectrum according to code.

Linear scaling procedure of the accelerograms does not affect the response given the spectral restraint provided by code's prescriptions (see [35] for details). Ground motion sets are composed of seven pairs of accelerograms, each one corresponding to North-South and East-West components of the same record. This choice allows considering mean seismic response of the seven analyses. Reference elastic response spectra for limit state of SD and DL are determined according to the Italian code [16].

In this case study, Significant Damage and Damage Limitation elastic response spectra are determined for the site (lat. 40.8249; long. 14.1891), assuming a life cycle of 50 years, C soil class, flat topography conditions. Rexel 3.5 software [36] is employed for the selection of spectrum-compatible accelerograms. Linear amplitude scaling procedure is employed to reduce dispersion of accelerograms' elastic spectra with respect to the target code spectra [35]. Accelerograms are selected from the European Strong Motion Database (ESD, http://www.isesd.hi.is/), in a range of magnitude (M) 6 to 7.5, and a range of epicentral distances (R) 0 to 50 km. The average scale factor (SF_m) of each set is limited to 2. In Figures 10, the fourteen 5% damped spectra of both horizontal components of the records selected, mean spectra, and tolerance bandwidths assumed are shown for the two limit states.

SD-LS and DL-LS data sets have six records in common, but different scale factors are applied to match the two different design spectra. Table 2 provide information on the accelerograms selected, while, in Table 3, scale factors, employed for each record and each limit state, are shown.

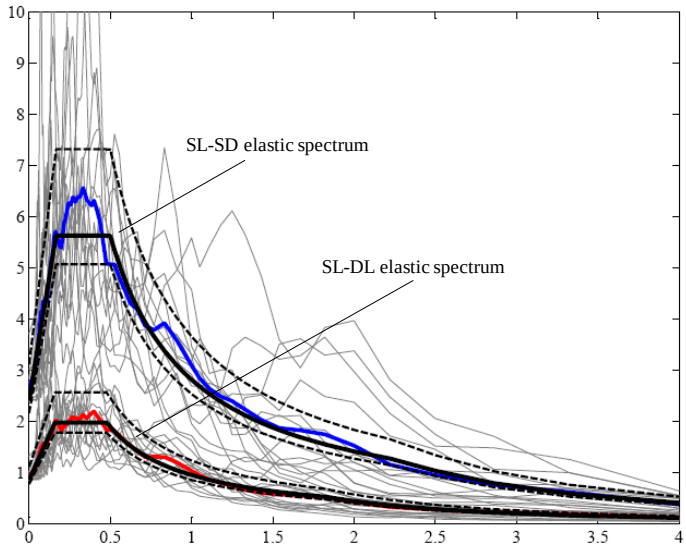

Figure 10. Sets of records: severe damage (SD) and damage limitation (DL)

Table 2. Records' information: waveform, earthquake ID in ESD, earthquake name, magnitude (M), fault mechanism, epicentral distance (R), and fault distance (R_{JB}).

Waveform ID	**Earthquake ID**	**Earthquake name**	**M**	**Fault mechanism**	**R** [km]	**R_{JB}** [km]
000074	43	Gazli	6.7	thrust	11	4
000170	81	Basso Tirreno	6.0	oblique	18	13
000175	83	Volvi	6.2	normal	29	13
000333	157	Alkion	6.6	normal	20	10
000335	158	Alkion	6.3	normal	25	19
000439	213	Spitak	6.7	thrust	36	20
000602	286	Umbria-Marche	6.0	normal	27	21
000879	349	Dinar	6.4	normal	8	0

Table 3. Scaling factors (SF) assumed the two record sets for Significant Damage (SD-LS) and Damage Limitation Limit States (DL-LS).

SD-LS				**DL-LS**			
NS	**SF_{NS}**	**EW**	**SF_{EW}**	**NS**	**SF_{NS}**	**EW**	**SF_{EW}**
000074	0.40824	**000074**	0.40015	**000074**	0.14484	**000074**	0.14197
000170	3.3295	**000170**	1.5103	**000170**	1.1813	**000170**	0.53582
000333	1.0605	**000333**	0.78818	**000333**	0.37625	**000333**	0.27963
000335	2.4117	**000335**	2.1498	**000335**	0.85564	**000335**	0.76271
000439	1.3346	**000439**	1.3326	**000439**	0.47348	**000439**	0.4728
000602	3.2401	**000602**	2.5728	**000602**	1.1495	**000602**	0.9128
000879	1.0121	**000879**	0.96242	**000175**	0.64843	**000175**	0.61441

Given the complexity of the nonlinear model of the Tower, the choice of the integration method aimed at performing nonlinear dynamic analysis was a key issue. Direct numerical integration approach and Hilber Hughes and Taylor integration method was employed, [37]; 1% mass and stiffness proportional damping was assumed. The latter assumption implies that coefficients of mass and stiffness matrix used to characterize damping matrix have negligible effects on the differences in results between bare and infilled nonlinear models of the structure; most of structural damping is assumed to be dissipated via hysteretic behavior of elements [38]. It is worth noting that no consideration on energy dissipation target are provided in EC8 [8], and the only peak response is accounted for in code approaches. The Eurocode-based assessment is

provided for both bare frame nonlinear model and tuff infilled nonlinear model in the cases of SD-LS and DL-LS.

4.1 EDP, capacities and IM-EDP response

Maximum interstorey drift ratio (MIDR) is the engineering demand parameter (EDP) chosen to characterize the seismic response of the Tower. MIDR is evaluated for all the storeys of the structure, with the exception of the first storey because of stairs' restraints (see section 3). The IDR is evaluated in four points at each level (see Figure 11). Joints A, B, C, and D are chosen to check both translational and torsional effects at each storey.

Seismic capacities are evaluated according to EC8 definition for each limit state considered. SD-LS seismic capacity is evaluated at the first attainment of 75% θ_u in the RC elements of the building, while DL-LS capacity is evaluated at the attainment of θ_y. This definition is adopted for both bare and infilled frame models. It is worth noting that, in the case of DL-LS, capacity evaluation of the infilled model could have been assumed according to a different criterion with respect to that of the bare model. One of the possible approaches is to consider the first attainment of the peak strength in the infill elements (e.g., [39]). On the other hand, given the specific distribution of the infills in the building, no difference in capacity is assumed. Thus, in the following, capacity of each element, and, in turn, of each storey (assumed as the minimum chord rotation capacity of the columns at the considered storey for SD-LS) is ruled by the only RC elements.

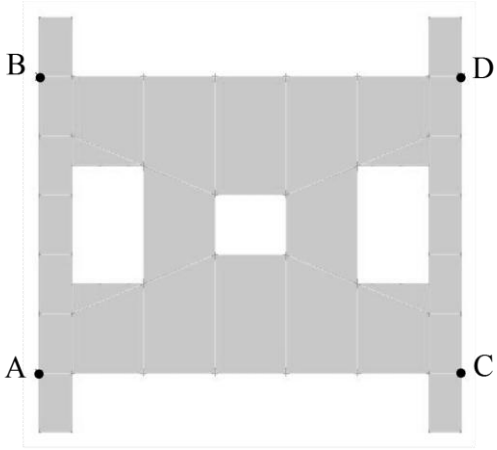

Figure 11. Joints A, B, C, and D for which IDR response is characterized.

Significant Damage capacities tend to increase with the height of the structure because of decreasing axial load in columns (ν), and decreasing section height (h), see equation 2. *Damage Limitation* capacities are similar at each level of the structure and amount approximately to 0.5%, corresponding to the value provided for existing buildings in the Italian Code ([16], [17]).

A common way to represent results of nonlinear analyses is to choose the Intensity Measure (IM) and plot analysis results in IM-EDP plane (Figure 12). $S_a(T_{el})$ is the chosen IM. The abscissa in Figure 12 is represented by the mean of the peak responses, in terms of MIDR, at the four joints represented in Figure 11. It is worth noting the significant differences between X and Y direction responses.

In Figure 12a and 12c, it can be observed that IMs for X direction are very similar for bare and infilled model; in fact in this direction no tuff infills are present and periods are very close for bare and infilled model (see Table 1).

On the other hand, comparison of bare and infilled responses, in Y direction (see Figure 12b and 12d), emphasizes how infilled model is characterized by lower MIDR demand with respect to the bare model at a given IM level. In particular, DL-LS results show that, in terms of medium response, infills provide a lower value of MIDR and a higher dispersion. The observed trend of the dispersion is the result of additional elements with nonlinear behavior in the model (i.e., infills).

Six of seven records show lower MIDR in the infilled model with the exception of record 000335 in which infilled model shows a value of MIDR equal to 0.69% and bare model a value of 0.38%. SD-LS results show, as well as DL-LS results, a lower mean value of MIDR in the infilled model and a remarkable difference in terms of standard deviation; $\sigma_{infilled}$ is equal to 0.60 and σ_{bare} is 0.25. Coefficients of variation (C.o.V) are equal to 0.55, in the infilled model, and to 0.20, in the bare model. In Y direction, two records, 879 and 335, provide MIDRs for the infilled model equal to 1.90% and 1.92%, respectively higher than the corresponding values in the bare model, 1.47% and 1.60% respectively. MIDR, in X direction, occurs at ninth level for bare and infilled model, and for both DL-LS and SD-LS analyses. In Y direction, DL-LS and SD-LS analyses show that tuff infills influence the storey at which MIDR occurs; infilled model attain MIDR at lower levels with respect to the bare model.

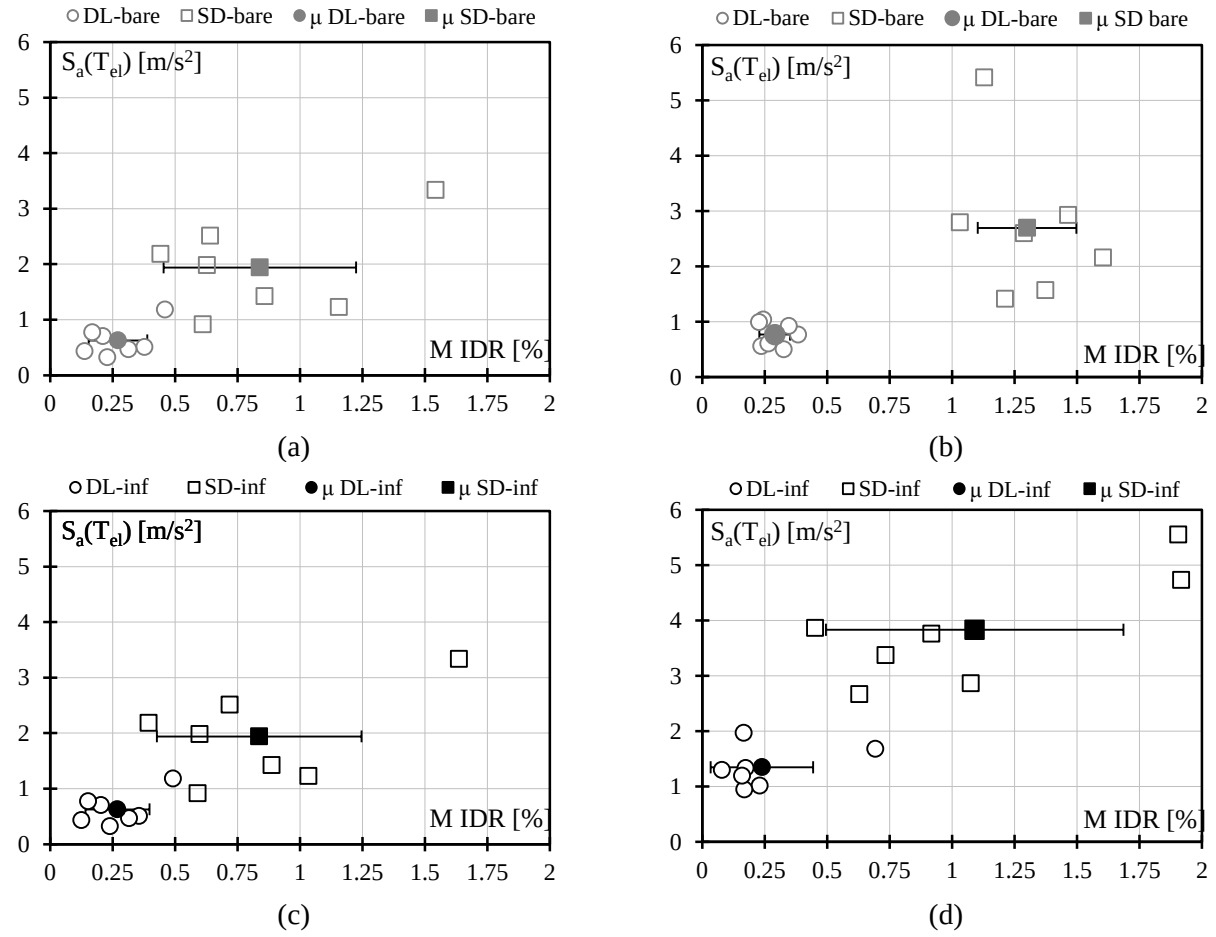

Figure 12. IM-EDP results for the bare model in X direction (a), and Y direction (b), and for the infilled model in X direction (c), and Y direction (d).

4.2 Significant Damage Limit State (SD-LS)

SD-LS results for X and Y directions, for bare and infilled model, are summarized in Figure 13; the maximum MIDR response at each storey, between the four joints considered, is shown. Results in Figure 13 represent the envelope of MIDR at each storey; the MIDR represented for each storey are attained at different time steps.

Torsional effects on the structure are different between X and Y direction. In X direction, for both bare and infilled model, the ratio between the maximum drift and the drift of the centre of the masses does not exceed 10% at each storey. In Y direction, drift increase up to 40% in the bare model and up to 35% in the infilled model. Maximum torsional effects (in Y direction) occur at eighth level in both bare and infilled model. Tuff infills reduce torsional effects in Y direction modifying stiffnesses' distribution in plan and elevation. As expected, MIDR have no substantial changes between bare and infilled model in X direction.

Results of Y direction for the bare model allow observing the effect of concrete braces (see Figures 2 and 6). In Y direction, for tuff infilled model, MIDR values are lower. In fact, tuff infills still tend to reduce MIDR profile at SD-LS.

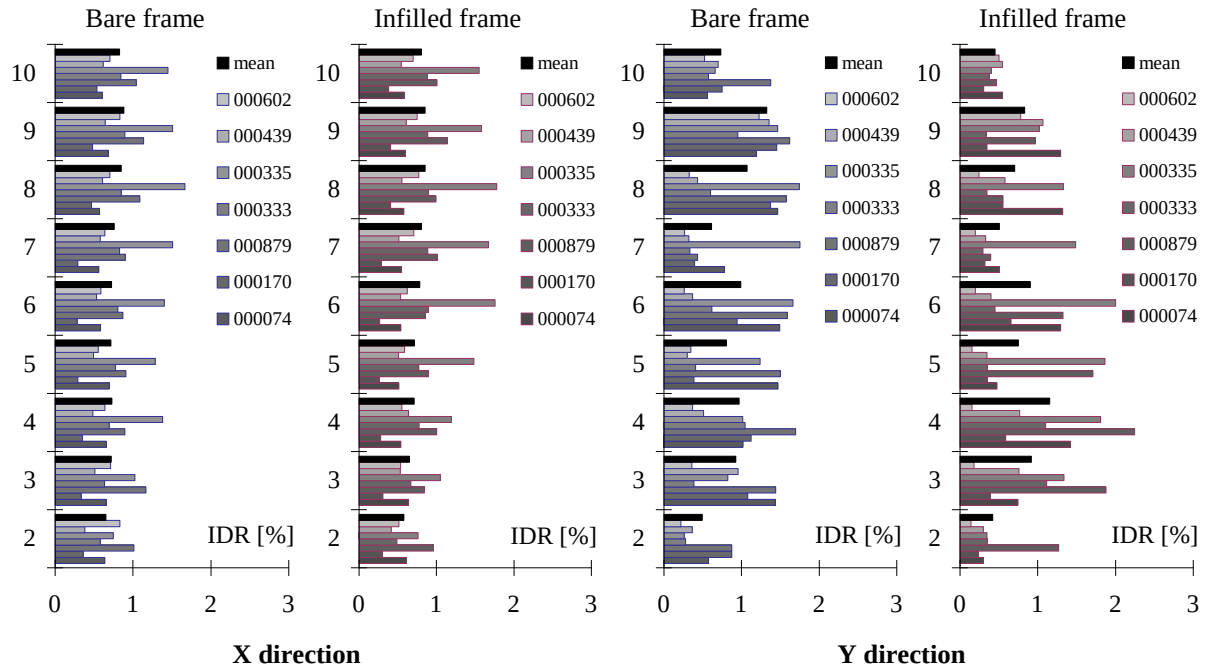

Figure 13. X and Y direction SD-LS, M IDR envelope at each storey for bare and infilled frame, (storey form 2 to 9).

Tuff infills' structural contribution can be easily recognized at ninth and tenth storeys at which only two braces are present. At these two storeys infills reduce demand up to 60%. From mean results in Figure 13, comparing MIDR of the two models, in Y direction, it can be seen that, in the infilled model, MIDR at fourth storey exceeds significantly that of the bare model. On the other hand, the average value of MIDR over the ten storeys is comparable.

Tuff infill, given their typical mechanical characteristics, can be considered "weak infill" according to the definition provided in Dolsek and Fajfar [40] and Verderame et al. [41]. In ordinary RC existing buildings, it could be expected that weak infills slightly reduce drift demand over the storeys. Nevertheless, at bottom storeys, the drifts of the infilled frame can be even larger than the bare corresponding frame [40]. According to the above general observations, fourth level can be considered as a bottom storey.

Given the complexity of the building, and the fact that the scattered configuration of storeys does not allow to assume a rigid diaphragm at each storey, it was chosen to represent the displacement profiles of two opposite verticals (along a diagonal) of the building at the attainment of MIDR (see Figures 14 and 15). The two verticals are A and D according to the scheme provided in Figure 11. For ultimate limit states, such as SD-LS, the plots in Figure 14 and 15 provide information on the inelastic deformed shape at peak demand for each single record considered, and 16%, 50%, and 84% percentiles of such displacement profiles show the storeys for which there is a concentration of inelastic demand.

Displacement profiles in X direction, for both bare and infilled models, and for verticals A and D (see Figures 14 and 15), have very similar trends: the deformed shape can be defined as a first mode shape, demand is comparable at each storey, and peak MIDR is attained for most records at eighth and ninth storeys. Record 170 is the only one that shows a change of sign in the deformed shape; it means that its frequency content amplifies the effects of higher modes. Notwithstanding the fact that displacement profiles in direction X are very similar for verticals A and D, the comparison of Figures14 and 15 emphasizes the presence of torsional effects. As an example, demand concentration at eighth and ninth storeys is more evident for vertical D (Figure 15) with respect to vertical A (Figure 14).

The comparison of displacement profiles in Y direction for bare and infilled model at the two verticals considered provides an informative overview of the changes in concentration of inelastic demand, and a confirmation of the reduction of torsional effects for the infilled model with respect to the bare, already observed from MIDR envelopes (see Figure 13). Infills, other than concentrating demand at bottom storeys (fourth) provide regularization in the deformed shape in Y direction. Figure 14 and 15 emphasizes the beneficial role that tuff masonry infills plays in this modern heritage structure, in fact, the bare model is characterized by a strict demand concentration at eighth and ninth storeys. The trend of demand amplification, already observed form MIDR envelopes is confirmed by the displacement profiles.

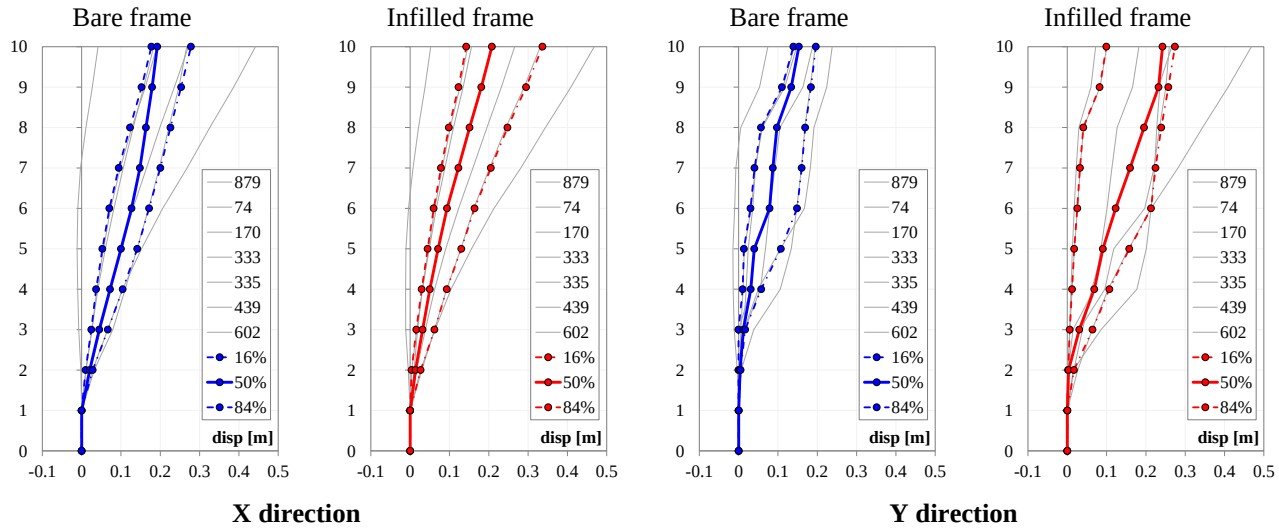

Figure 14. X and Y direction SD-LS, displacement profiles at the attainment of MIDR for bare and infilled frame at the control vertical A (see Figure 11).

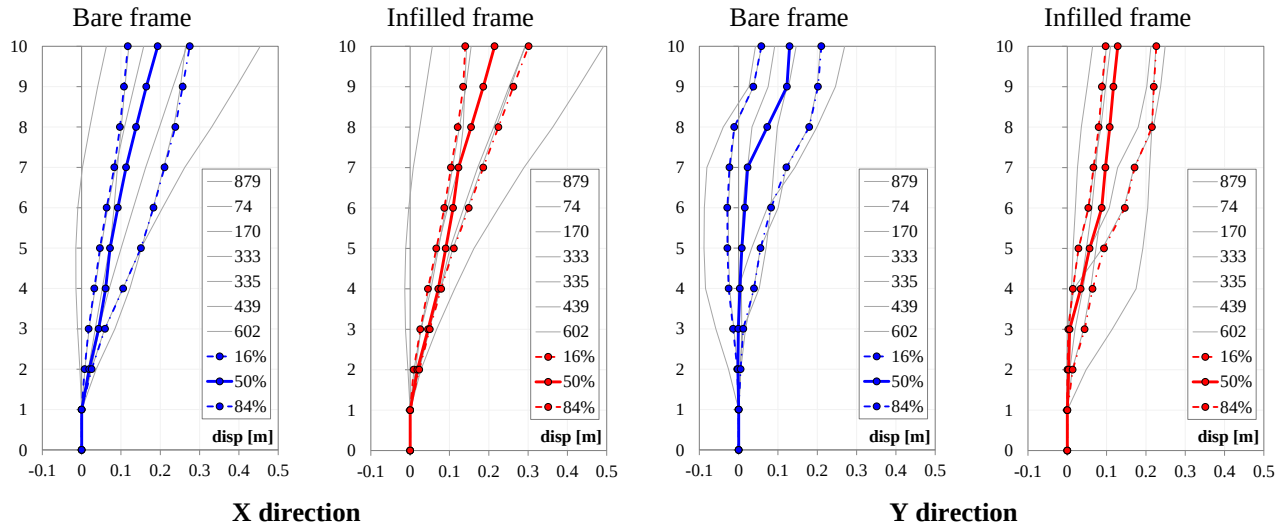

Figure 15. X and Y direction SD-LS, displacement profiles at the attainment of MIDR for bare and infilled frame at the control vertical D (see Figure 11).

The above observations can be specialized considering single record trends in terms of MIDR and roof drift ratio (RDR). Results from every single couple of accelerograms emphasize the large scattering in terms of MIDR results. In X direction, record 335 shows the most severe response for both bare and infilled model. In Y direction of bare model, record 879 provides the most severe response. While record 335 is the one showing the most severe response for infilled model in Y direction.

Considering the differences in the first period between bare and infilled frame, in Y direction, the same record can have very different responses. Figure 16 shows time history results, for record 335, in terms of RDR for both bare and infilled models in X and Y directions. Comparison of RDR

response for record 335, in Y direction, emphasizes a negligible difference between bare and infilled model (see Figure 16). On the other hand, results for the same record in terms of MIDR at each storey show that, locally, drift distribution is characterized by significant differences (see as an example, the response of fourth storey for record 335 in Figure 13).

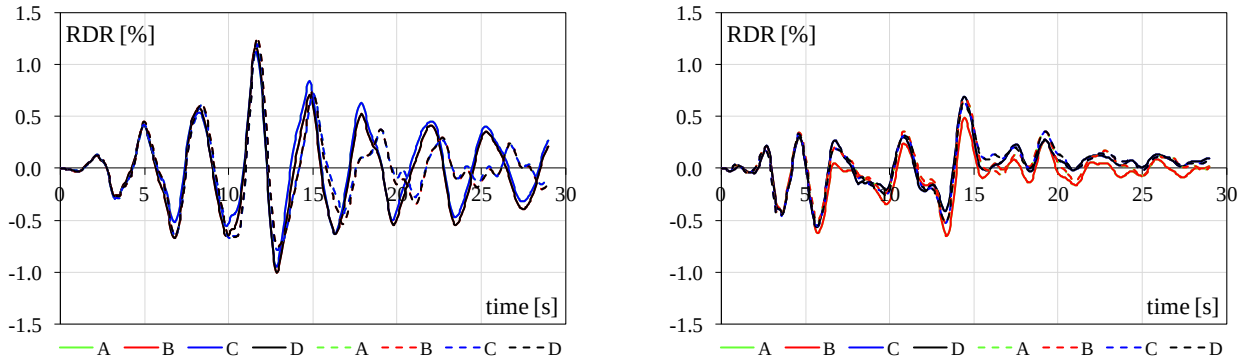

Figure 16. Roof drift ratio (RDR) at the joints A, B, C, and D for record 335 in the case of SD-LS for bare (solid lines) and infilled (dashed lines) models in (a) X direction, and (b) Y direction

Figure 17 shows assessment results for SD-LS in the two principal directions for both bare and infilled model. The structure is safe according to EC8 in both the modeling hypotheses with similar ρ ratios (IDR demand over IDR capacity at each storey). Y direction shows higher ρ ratios than X direction. Bare model in Y direction has the maximum ρ mean ratio at the ninth level (0.75), while tuff infilled model attains maximum ρ at the fourth storey (0.83). The effect of tuff infills changes local damage distribution and consequently ρ ratios along the height of the Tower.

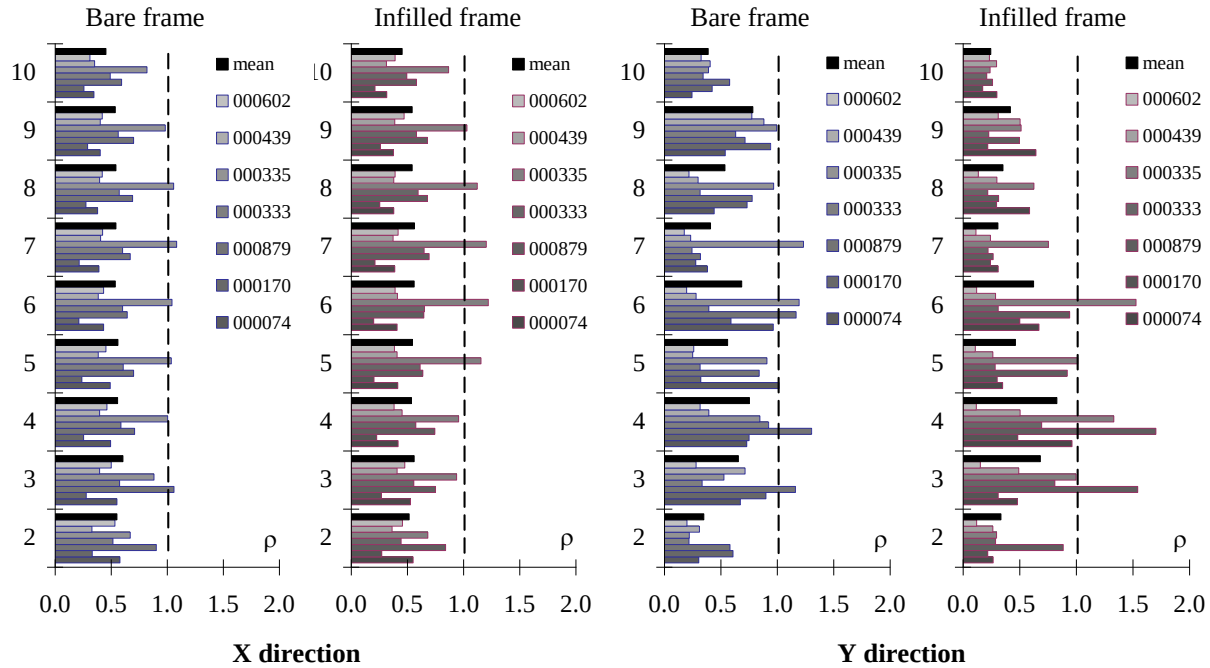

Figure 17. X and Y direction SD-LS: ρ ratio bare and infilled frame, (storey form 2 to 9).

4.3 Damage Limitation Limit State (DL-LS)

Maximum responses in terms of MIDR at each storey between the four joints considered appear in Figure 18. Results in Figure 18 represent the envelope of MIDR at each storey; the MIDR represented for each storey are attained at different time steps. In X direction, there are no significant differences between bare and infilled model in accordance with SD-LS results. In Y direction, it is possible to recognize the effect of tuff infillings that decreases strictly IDR demand.

In accordance with SD-LS results, tuff masonry infills change the storey at which the maximum IDR occurs: for bare model, it is the ninth, for infilled one, it is the fourth.

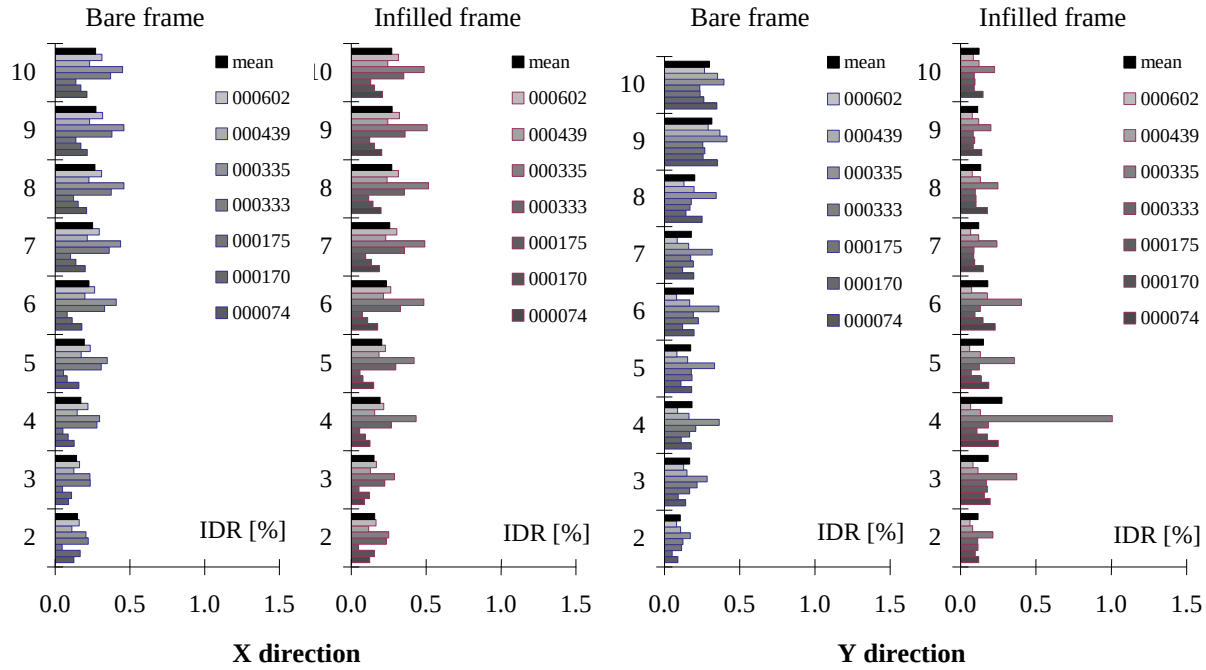

Figure 18. X and Y direction DL-LS, M IDR envelope at each storey for bare and infilled frame, (storey form 2 to 9).

Record 335 has the most severe response in both directions and for both models. At the fourth storey of the infilled model, this record causes the highest MIDR (1%). This MIDR demand exceeds significantly the IDR correspondent to the maximum strength point of infillings and consequently leads to complete crushing of the infillings at this level. Time history results, for record 335, in terms of roof drift ratio (RDR) for both bare and infilled models in X and Y directions are presented in Figure 19. Comparison of RDR response for record 335, in Y direction, emphasizes a more significant difference between bare and infilled model with respect to the same results shown for the case of SD-LS. Again, local MIDR response is strictly affected by infills, while values of RDR emphasize that RDR is not strictly affected by infills.

The structure is safe according to EC8 for both the modeling hypothesis. Figure 20 shows ρ ratio (IDR demand over IDR capacity) for the model in the two directions. Bare model in Y direction has the maximum ρ mean ratio at the tenth storey (0.93), tuff infilled model have the maximum at the fourth storey (0.44). Trends in Figure 20 reflect the observed trends in terms of MIDR, given the assumption that capacity for DL-LS does not change when considering tuff infills. The effect of tuff infills changed completely the evaluation of local damage and the value of the ratio between demand and capacity.

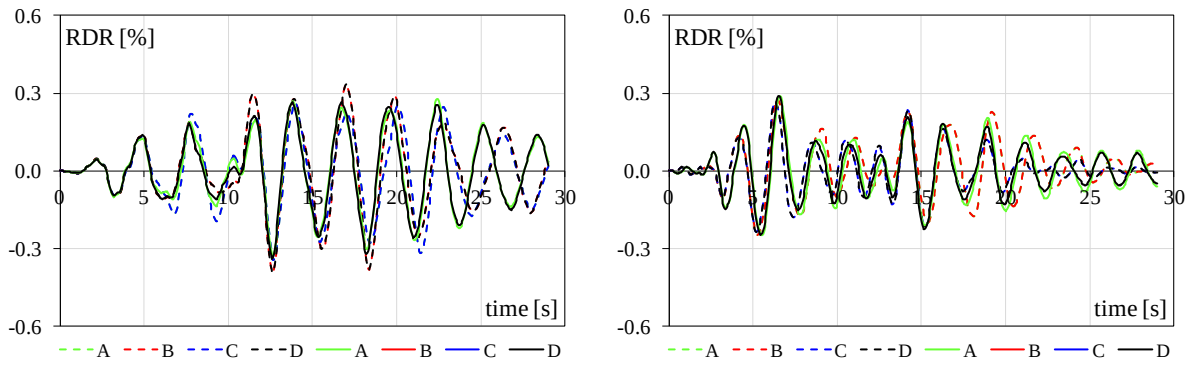

Figure 19. Roof drift ratio (RDR) at the joints A, B, C, and D for record 000335 in the case of LS-DL for bare (solid lines) and infilled (dashed lines) models in (a) X direction, and (b) Y direction

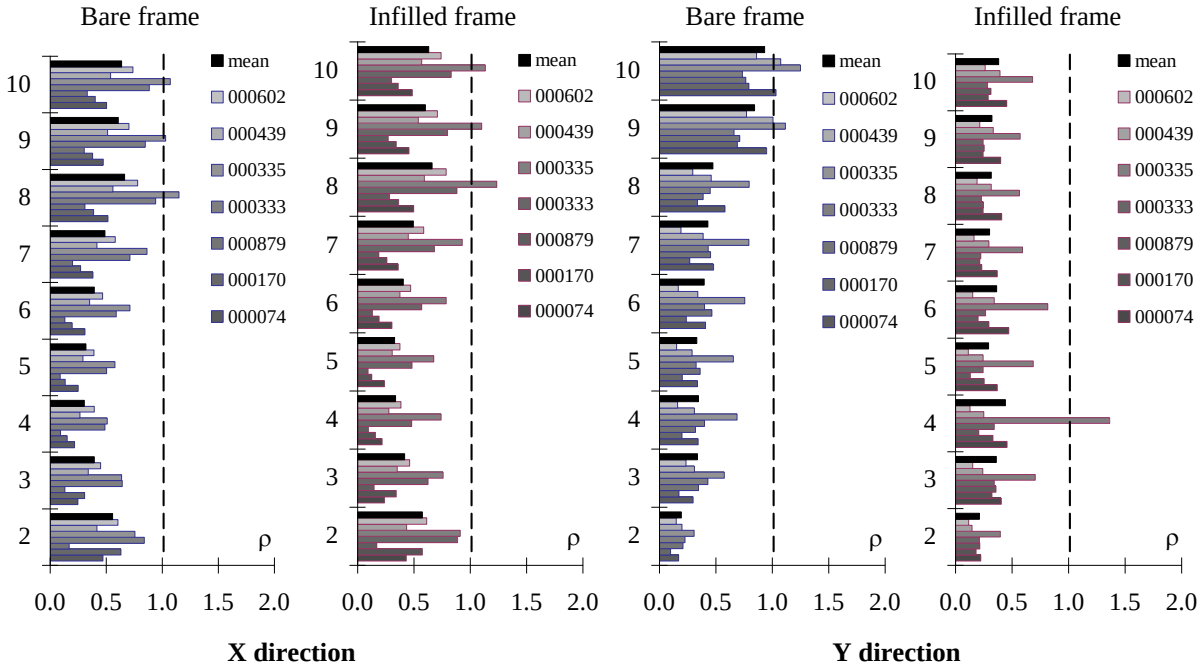

Figure 20. X and Y direction LS-DL: ρ ratio bare and infilled frame, (storey form 2 to 9).

Notwithstanding the limited contribution in terms of strength and stiffness provided by tuff infills with respect to typical brick masonry infills (e.g., [39], [41]), they still provide an important contribution in limiting demand when DL-LS is of concern. On the other hand, if a different capacity criterion had been assumed for the infilled model, i.e. the first attainment of peak displacement in the infills of each storey, the above considerations would have been completely different. In fact, the counterpart of the demand decrease observed in the infilled model would have been overtaken by a significant decrease in capacity whose amount, in terms of IDR (approximately equal to 0.05%), would have been of one order of magnitude lower.

The above results emphasize how DL-LS can be strictly affected by the specific capacity assumptions made when performing the assessment of the building, and how such assumptions need to be adapted to the specific peculiarities of the structure in the case of modern heritage structures.

5. CONCLUSIONS

Given the interest earned recently by modern heritage structures, seismic assessment criteria of Eurocode 8 for ordinary reinforced concrete structures are applied to a modern heritage RC building. This case study, the Tower of the Nations in Naples, was designed in 30's, and represents one of the first important RC structures realized in Italy. *In situ* inspections and testing provided the necessary knowledge of the structure in terms of geometry, structural details, and material properties. In particular, it is a ten-storey building with staggered configuration of the floors in elevation, two façades have a concrete bracing system and tuff masonry infills, and the other two are glazed façades.

Two nonlinear models of the structure are built up in both the hypotheses of accounting and not accounting for tuff infills' stiffness and strength contribution. Lumped plasticity model for reinforced concrete elements and equivalent strut macro model for tuff and concrete infills are employed. Modeling issues regarding concrete braces and slim concrete infills are overtaken considering literature results that provide a pursuable approach for these peculiar elements.

Seismic assessment through nonlinear dynamic analyses is carried out for both limit states of Significant Damage and Damage Limitation. Seismic input is selected according to EC8 and Italian Seismic code, making use of proper sets of seven pairs of scaled recorded accelerograms, (seven per each principal direction of the building).

Capacities are evaluated according to EC8 definition for each limit state considered. SD-LS capacity is evaluated at the first attainment of 75% θ_u in the RC elements of the building, while DL-LS capacity is evaluated at the attainment of θ_y. This definition is assumed for both bare and infilled model. The latter assumption, different from the approach typically adopted for ordinary RC buildings, is justified by the specific distribution of the infills on the Tower: all located along one single direction.

Seismic assessment of bare and infilled models emphasizes:

- lower demand in terms of maximum interstorey drift of the infilled model with respect to the bare, for both limit states considered. Scattering around the mean values evaluated on the sets of seven records becomes significantly larger if infills contribution is taken into account;
- outcome of the assessment is not affected by infills, i.e. the structure can be considered safe for both limit states, and in both modeling hypotheses. On the other hand, the ratio demand over capacity, for both the limit states considered, is strictly influenced by infills' contribution.

Finally, results highlight that tuff masonry infill increases stiffness and strength of the building as long as the seismic demand does not exceed the deformation capacity of the infillings; after that, both global stiffness and global strength deteriorate. On the other hand, displacement profiles show that tuff infills provide a regularization of demand along the height of the building. Therefore, non-structural elements contribution still plays a significant role in the assessment, even in the case of modern heritage RC structures in which materials employed are not conventional, e.g., tuff rather than clay hollow bricks.

Non-destructive tests and experimental evaluation of dynamic properties (modal identification of the structure) represent a useful benchmark to test modeling approaches and reliability of the assumptions made. Assessment tools provided for ordinary RC structures can be addressed to modern heritage buildings as shown in this case study, even if specific care is necessary for nonlinear structural modeling in case of non-conventional structural elements.

REFERENCES

[1] Vecco M. A definition of cultural heritage: from the tangible to the intangible. Journal of Cultural Heritage, 2010; 11:321-324.

[2] Augusti G., Ciampoli M. Heritage buildings and seismic reliability. Progress in Structural Engineering and Materials, 2000; 2:225-237.

[3] Gülkan P., Wasti S.T. Seismic assessment and rehabilitation of historic structures. Structural Longevity, 2009; 1(2):111-134.

[4] Ronca P., Franchi A., Migliacci A. Open issues for the conservation of land-mark modern architecture. Protection of Historical Buildings, PROHITECH 09 – Mazzolani (ed), Taylor and Francis Group, London, ISBN 978-0-415-55803-7, 2009.

[5] Mosoarca M., Victor G. Structural safety of historical buildings made of reinforced concrete, from Banat region – Romania. Journal of Cultural Heritage, 2009; 14S:e29-e34.

[6] Syrmakezis C.A. Seismic protection of historical structures and monuments. Structural control and health monitoring, 2006; 13:958-979.

[7] Ministero dei Beni e le Attività Culturali. Linee Guida per la valutazione e riduzione del rischio sismico del patrimonio culturale allineate alle nuove Norme tecniche per le costruzioni (D.M. 14 gennaio 2008), Circolare 26/2010, 2010, (in Italian).

[8] Comitè Europèen de Normalisation. Eurocode8, Design of Structures for earthquake resistance – Part3: Assessment and retrofitting of buildings. EN 1998-1, CEN, Brussels, 2005.

[9] Siola U. La Mostra d'Oltremare e Fuorigrotta, Electa, Napoli, 1990, (in Italian).

[10] Regio Decreto 27/07/1933 n.1213. Prescrizioni regolamentari italiane per l'esecuzione delle opere in cemento armato, G.U. n.224, 26/09/1933, 1933, (in Italian).

[11] Regio Decreto 16/11/1939 n. 2229. Norme per la esecuzione delle opere in conglomerato cementizio semplice e armato, G.U. n. 92, 18/04/1940, 1939, (in Italian).

[12] Verderame G.M., Polese M., Mariniello C., Manfredi G. A simulated design procedure for the assessment of seismic capacity of existing reinforced concrete buildings. Advances in Engineering Software, 2010; 41:323–335.

[13] Manfredi G., Masi A., Pinho R., Verderame G.M., Vona M. Valutazione degli edifici esistenti in cemento armato. IUSS Press, Pavia, Italy, 2007, (in Italian).

[14] Computers and Structures. SAP 2000. Linear and nonlinear static and dynamic analysis and design of three dimensional structures. CSi, Berkeley, California, 2007.

[15] Rainieri C., Fabbrocino G., Verderame G.M. Non-destructive characterization and dynamic identification of a modern heritage building for serviceability seismic analyses. NDT & E International, 2013; 60:17-31.

[16] DM 14 Gennaio 2008. Norme tecniche per le costruzioni. Gazzetta Ufficiale della Repubblica Italiana, 29, 2008, (in Italian).

[17] CS.LL.PP.; 617/2009. Istruzioni per l'applicazione delle norme tecniche delle costruzioni. Gazzetta Ufficiale della Repubblica Italiana, 47, 2009, (in Italian).

[18] Mander J.B., Priestley M.J.N., Park R.. Theoretical Stress-Strain Model for Confined Concrete. Journal of Structural Engineering, 1988; 114(8):1804-1826.

[19] Biskinis, D.E. and Fardis M.N. Deformations at flexural yielding of members with continuous or lap-spliced bars. Structural Concrete, 2010; 11(3): 127-138.

[20] Biskinis D.E. and Fardis MN. Flexure-controlled ultimate deformations of members with continuous or lap-spliced bars. Structural Concrete, 2010; 11(2): 93-108.

[21] Verderame G.M., Ricci P., Manfredi G. Ultimate chord rotation of RC columns with smooth bars: some considerations about EC8 prescriptions. Bulletin of Earthquake Engineering, 2010;8:1351-1373.

[22] Verderame G.M., Fabbrocino G., Manfredi G. Seismic response RC columns with smooth reinforcement- PART1- Monotonic tests. Engineering Structures, 2008; 30(9):2277-2288.

[23] Verderame G.M., Fabbrocino G., Manfredi G. Seismic response RC columns with smooth reinforcement- PART2- Cyclic tests. Engineering Structures, 2008; 30(9):2289-2300.

[24] Di Ludovico M., Verderame G.M., Prota A., Manfredi G., Cosenza E. Cyclic Behavior of Nonconforming Full-Scale RC Columns, Journal of Structural Engineering, ASCE, 2013; DOI: 10.1061/(ASCE)ST.1943-541X.0000891.

[25] Takeda T, Sozen MA, Nielsen NN. Reinforced concrete response to simulated earthquakes. Journal of Structural Engineering Division, 1970; 96(12):2557–2573.

[26] Dowell R.K., Seible F., Wilson E.L. Pivot Hysteresis Model for Reinforced Concrete Members. ACI Structural Journal, 1998; 95(5):607-617.

[27] De Luca F., Verderame G.M. A practice-oriented approach for the assessment of brittle failures in existing RC elements, Engineering Structures, 2013; 48:373-388.

[28] Corradi Dell'Acqua L. Meccanica delle Strutture- La valutazione della capacità portante - vol. III. McGraw-Hill, Milan, 1994, (in Italian).

[29] Fardis M.N., Panagiotakos T.B. Seismic design and response of bare and masonry-infilled reinforced concrete buildings Part II, infilled structures. Journal of Earthquake Engineering, 1997; 1(3):475–503.

[30] Mainstone R.J. Supplementary note on the stiffness and strength of infilled frames. Current paper CP13/74. Building Research Establishment, London, 1974.

[31] Al-Chaar G., Issa M., Sweeney S. Behavior of Masonry-Infilled Nonductile Reinforced Concrete Frames. ASCE Journal of Structural Engineering, 2002; 128(8):1055-1063.

[32] Kara M.E., Altin S. Behavior of Reinforced Concrete Frames with Reinforced Concrete Partial Infillings. ACI Structural Journal, 2006; 103(5):701-709.

[33] Anil Ö., Altin S. An Experimental study on reinforced concrete partially infilled frames. Engineering Structures, 2007; 29:449-460.

[34] Comitè Europèen de Normalisation. Eurocode8. Design of Structures for earthquake resistance – Part1: General rules, seismic actions and rules for buildings, EN 1998-1, CEN, Brussels, 2004.

[35] Iervolino I., De Luca F., Cosenza E. Spectral shape-based assessment of SDOF nonlinear response to real, adjusted and artificial accelerograms. Engineering Structures, 2010; 32:2776-2792.

[36] Iervolino I., Galasso C., Cosenza E. REXEL: computer aided record selection for code-based seismic structural analysis. Bulletin of Earthquake Engineering, 2010; 8(2):339-362.

[37] Wilson E.L. Three Dimensional Static and Dynamic Analysis of Structures. CSi Berkeley, California, 2002.

[38] Elnashai A.S., Di Sarno L. Fundamentals of Earthquake Engineering. John Wiley & Sons, 2008.

[39] Dolšek M., Fajfar P. The effect of masonry infillings on the seismic response of a four storey reinforced concrete frame – a deterministic assessment. Engineering Structures, 2008, 30(7), 1991-2001.

[40] Dolšek M., Fajfar P. Soft storey effects in uniformly infilled reinforced concrete frames. Journal of Earthquake Engineering, 2001; 5(1):1-12.

[41] Verderame G.M., De Luca F., Ricci P., Manfredi G. Preliminary analysis of a soft storey mechanism after the 2009 L'Aquila earthquake. Earthquake Engineering and Structural Dynamics, 2011; 40(8):925–44.